

# Opportunities for chiral discrimination using high harmonic generation in tailored laser fields

Olga Smirnova<sup>1</sup>, Yann Mairesse<sup>2</sup>, Serguei Patchkovskii<sup>1</sup>

<sup>1</sup> Max-Born Institute for Nonlinear Optics and Short Pulse Spectroscopy,  
Max-Born-Strasse 2A, D-12489 Berlin, Germany

<sup>2</sup> CELIA, Université de Bordeaux - CNRS - CEA, F33405 Talence, France

**Abstract.** Chiral discrimination with high harmonic generation (cHHG method) has been introduced in the recent work by R. Cireasa et al (*Nat. Phys.* **11**, 654 - 658, 2015). In its original implementation, the cHHG method works by detecting high harmonic emission from randomly oriented ensemble of chiral molecules driven by elliptically polarized field, as a function of ellipticity. Here we discuss future perspectives in the development of this novel method, the ways of increasing chiral dichroism using tailored laser pulses, new detection schemes involving high harmonic phase measurements, and concentration-independent approaches. Using the example of the epoxypropane molecule  $C_3H_6O$  (also known as 1,2-propylene oxide), we show theoretically that application of two-color counter-rotating elliptically polarized laser fields yields an order of magnitude enhancement of chiral dichroism compared to single color elliptical fields. We also describe how one can introduce a new functionality to cHHG: concentration-independent measurement of the enantiomeric excess in a mixture of randomly oriented left-handed and right-handed molecules. Finally, for arbitrary configurations of laser fields, we connect the observables of the cHHG method to the amplitude and phase of chiral response, providing a basis for reconstructing wide range of chiral dynamics from cHHG measurements, with femtosecond to sub-femtosecond temporal resolution.

Submitted to: *J. Phys. B: At. Mol. Opt. Phys.*

## 1. Introduction

Ever since their discovery, chiral molecular systems puzzled and inspired researchers. The mirror symmetry, characterizing two molecular enantiomers, is possibly the simplest broken symmetry to think of. The complexity and variety of interactions and occurrences in nature of different enantiomers, flowing from such a small difference in their structure, is amazing. Chiral nature of living matter poses both fundamental and practical questions, from the origins of homochirality in biomolecules [1] to detection and manipulation [2] of chiral properties. The oldest method used to detect chirality in such media is optical rotation: the polarization plane of a linearly polarized light propagating through left and right chiral media rotates in opposite directions (see e.g. optical rotation measurement in epoxypropane molecule; we shall use this molecule to illustrate our concepts here [3]),

Microscopically, optical rotation is governed by the interplay of dipole transitions in a chiral medium caused by electric and magnetic fields of a light wave. While the electric transition dipoles are identical in the two enantiomers in their respective molecular frames, the magnetic dipoles are pointing in opposite directions leading to opposite dynamical electronic response in the two enantiomers. The same mechanism underlies other linear chiroptical techniques which use circularly polarized light to detect differences in absorption (circular dichroism), Raman scattering, or circular fluorescence [4] between the two enantiomers. It is useful to note that while chirality is a topological property of molecular structure, chiral response to light is caused by chiral electronic dynamics, which thus effectively 'measures' this structural property.

Weak magnetic effects lead to weak chiroptical response. For example, circular dichroism is often three to six orders of magnitude smaller than light absorbance at the same wavelength. Weakness of chiral response poses challenges for time-resolved measurements of chiral dynamics.

One way of increasing chiral response is to employ techniques that do not rely on weak interaction with the magnetic field component of the electromagnetic wave, such as e.g. photoelectron spectroscopy [5], microwave detection [6], or Coulomb explosion imaging [7]. Two of these techniques, one-photon [8, 9, 10] and multiphoton [11, 12, 13] photoelectron circular dichroism (PECD) are pertinent to the approaches to chiral discrimination involving high harmonic generation (cHHG method [14]). In particular, one-photon ionization is the inverse of photorecombination, which is the key step in high harmonic generation.

The PECD detection requires resolving the direction of the final electron momentum: the photoelectron angular distribution obtained from randomly oriented chiral molecules shows asymmetry with respect to the direction of light propagation. This asymmetry originates from the electron interaction with the chiral potential of the core [8, 15], i.e. is the dynamical consequence of the chiral structure. The effect is most prominent for low energy electrons [16], since interaction with the chiral core potential is maximized in this case. The chiral dichroism signal achievable with PECD, up to

some 10%, sets the 'golden standard' for the cHHG method [14].

With the advent of ultrafast light sources, there has been an increasing interest in developing ultrafast chiroptical spectroscopic techniques to investigate chiral response in the time domain. In the condensed phase, several breakthroughs have been achieved [17, 18] using non-linear chiroptical spectroscopy [17, 18, 19, 20]. In the gas phase, where isolated compounds can be studied, such measurements are a lot more challenging due to low density of samples, so that no ultrafast measurement at  $\sim 10^1$  fsec time scale has yet been reported. High sensitivity of PECD may open a path towards such measurements, provided that ultrashort circularly polarized laser [11, 12, 13] or XUV pulses [21, 22] are used.

Importantly, cHHG naturally offers sub-femtosecond temporal resolution and allows one to detect multielectron chiral dynamics on their natural attosecond timescale. The chiral response can be monitored with  $\Delta t \sim 0.1$  fsec resolution [14], orders of magnitude better than achieved so far (see e.g. [23]). Moreover, already the first experiments [14] demonstrated very high enantio-sensitivity of the cHHG approach, leading to about 2-3% chiral signal for nearly linearly polarized laser fields, with ellipticity  $\epsilon \sim 1\%$ . Thus, cHHG may represent an exciting alternative to PECD for ultrafast studies in the gas phase. Here we discuss the opportunities for extending the first cHHG measurements [14] to increase their sensitivity and versatility, striving to turn cHHG into a standard ultrafast chiroptical detection technique.

High-harmonics generation (HHG) can be understood as a sequence of three steps [24, 25]: ionization in a strong laser field, laser-induced acceleration of the liberated electron, and its recombination with the parent ion, all within the same laser cycle. High harmonic generation spectroscopy can be viewed as a pump-probe technique. Ionization acts as a pump, simultaneously launching the continuum electron and the correlated multielectron dynamics in the cation. Recombination acts as a probe of such dynamics [26, 27, 28]. The pump-probe delay is controlled by light oscillation with attosecond precision; the ionization and emission times can be accurately characterised [29, 31, 32]. Effectively, the emitted light records a movie of the recombining system, with each harmonic representing a single frame [26, 27].

The ability to record multielectron dynamics on attosecond time-scale [27, 28] is one of the most exciting features of high harmonic spectroscopy. This multielectron dynamics can be visualised as the motion of a hole created in a molecule upon ionization. The shape, location, and momentum of the hole during recombination are mapped onto the properties of the emitted light - its amplitudes, phases, and polarizations [27, 33, 34, 35]. This link is crucial for cHHG.

Indeed, one of the effective mechanisms of chiral sensitivity of HHG is directly linked to attosecond laser-driven dynamics of the hole between ionization and recombination. Equivalently, one can think about laser-driven multi-electron dynamics in the molecular ion, i.e. light-induced transitions between its electronic states. Chiral sensitivity arises due to the interference of two types of transitions between the electronic states of the cation [14]: the electric dipole transitions driven by the minor component of the electric

field, and the magnetic dipole transitions driven by the major component of the magnetic field. This interplay of the magnetic dipole and electric dipole transitions occurs on the sub-cycle time-scale. The enantio-sensitive sub-cycle dynamics reflects the molecular structure, which dictates the strength of the strong-field driven chiral response. Note that this dynamics occurs with the nuclei still located at their positions in the neutral molecule: there is very little time for the nuclei to move during the fraction of the laser cycle between ionization and recombination.

Optimal regime for the interference of the magnetic dipole transition driven by the major component of the magnetic field and the electric dipole transition driven by the minor component of the electric field requires balance between the magnitudes of the respective interactions,  $|\mu H_0| \sim |\epsilon d E_0|$ . Here  $E_0 = H_0$  are the amplitudes of the electric and magnetic fields of the laser pulse,  $\mu$  is the matrix element of the magnetic dipole transition,  $d$  is the matrix element of the electric dipole transition,  $\epsilon$  is the ellipticity of the laser field,  $\epsilon E_0$  is the amplitude of the minor component of the electric field. Since  $|\mu| \sim 10^{-2}|d|$ , the balance is achieved for  $|\epsilon| \sim 1\%$ , i.e. for nearly linear fields. Since  $\vec{\mu}$  changes direction by  $180^\circ$  between the two enantiomers of the chiral molecule, constructive interference requires opposite values of helicity for right and left enantiomers, giving rise to chiral dichroism. Chiral dichroism at a few percent level for such almost linear fields observed in Ref. [14] demonstrates high potential for chiral discrimination of this new technique. However, as with any new technique, its first implementation may not be optimal.

The observed cHHG signal [14] maximises for very low ellipticities  $\epsilon \sim 1\%$ . On the one hand, the chiral response typically increases with increasing ellipticity, likely maximizing for circular rather than nearly linear fields. On the other hand, the harmonic signal drops quickly with increasing ellipticity. These conflicting requirements seem to preclude exploration of what could be a more favourable regime. Resolving this conflict should enhance sensitivity and flexibility of the cHHG technique.

Tailoring driving fields to maximize the chiral response and optimize the cHHG is a clear direction forward. Specifically, one should aim to (i) maximise effects of the chiral hole dynamics in the molecular ion between ionization and recombination, without sacrificing high harmonic generation efficiency; (ii) explore application of other tools of high harmonic spectroscopy to chiral discrimination, complementing measurements of the harmonic spectra with measurements of the harmonic phase [27, 28, 29, 30]. Below, we show how both aims can be achieved using tailored multicolor fields.

The use of multicolor, shaped fields for cHHG should allow one to achieve two important goals.

First, additional fields can couple ionic states populated during ionization to the ionic states not directly populated during the ionization step, but characterized by strong magnetic dipole transitions, for example due to the proximity of their respective orbitals to a chiral center. This would make the cHHG method truly general, applicable to many chiral molecules, even if the ionization step does not directly populate electronic states with strong magneto-dipole transitions.

Second, circular light has long been used to detect chiral response because such light has high chirality. However, the high harmonic yield maximises for linear fields and quickly drops with increasing  $\epsilon$ . Application of chiral multi-color fields resolves this problem. The family of counter-rotating two-color fields, introduced in [36], can combine circular or elliptic polarization with strong high harmonic response [22].

Here we consider the application of elliptic counter-rotating two-color laser fields,

$$E_1 = E_0(\epsilon_1 \cos(\omega t)\hat{e}_x + \sin(\omega t)\hat{e}_y), E_2 = E_0(\epsilon_2 \cos(2\omega t)\hat{e}_x - \sin(2\omega t)\hat{e}_y), \quad (1)$$

to induce, enhance and manipulate the chiral HHG response from randomly oriented gas of chiral molecules. In Eq.(1)  $E_0$  is the field strength,  $\epsilon_1, \epsilon_2$  are the ellipticities of the fundamental field and its second harmonic,  $\hat{e}_{x,y}$  are the unit vectors in the polarization (x,y) plane of the laser field.

Below, we theoretically show that application of such fields should allow one (i) to improve the sensitivity of the cHHG method to rival the sensitivity of the PECD measurements, without relying on using the driving light with very small ellipticity, (ii) to increase the range of harmonics for which the chiral signal is strong. We also show how phase measurements of the chiral high harmonic signal allow one to determine the amount of specific enantiomers (enantiomeric excess) in a mixture, in a way that does not require one to know the medium concentration. Finally, we present the theoretical background for the reconstruction of time-dependent chiral response for arbitrary ellipticities and configurations of the driving laser fields.

## 2. Chiral discrimination based on HHG spectral and phase measurements

In this section, we apply the approach we have already used in [14] to estimate the high harmonic signal vs ellipticity of the field given by Eq. (1). We set the ellipticities of both fields to be equal,  $\epsilon_1 = \epsilon_2 = \epsilon$ . We will consider an epoxypropane molecule  $\text{CH}_3\text{CHCH}_2\text{O}$  (also known as 1,2-propylene oxide), which has been used in the first cHHG experiments [14].

There are two key cHHG channels in strong field ionization of epoxypropane. These channels are associated with leaving the ion either in the ground electronic state  $X$  upon ionization, or in the first excited state electronic state  $A$ . In the former case, the returning electron can recombine with the ion in state  $X$ , in the latter case, with the ion in state  $A$ . Higher excited electronic states are well separated in energy from these two, and do not contribute to ionization in strong mid-infrared laser fields.

Recombination of the continuum electron with the parent ion in these states gives rise to direct HHG channels,  $XX$  and  $AA$ . Here the first letter marks the ionization channel and the last marks the recombination channel. Laser-induced transitions between the states  $X$  and  $A$  of the ion open additional cross-channels [35]:  $XA$  and  $AX$ . For example, strong field ionization can leave the ion in the state  $X$ , but laser-induced transitions can excite the ion to the state  $A$ . The returning electron now has to recombine with this state: the hole created in the molecule during ionization is different from the hole before recombination. This results in the  $XA$  channel in HHG.

Importantly,  $XA$  and  $AX$  are chiral sensitive since they involve the interference of the laser-driven electric dipole and magnetic dipole transitions [14]. Our calculations [14] show that ionization and recombination create strongly preferred direction for the  $A$  channel, while the ionization-recombination angular dependence for the channel  $X$  has no such preferred direction. Also, the cross-channel  $XA$  associated with the ionization to the channel  $X$  followed by recombination to the channel  $A$  is suppressed relative to the channel  $AX$ . Along the direction of maximal ionization for the channel  $A$ , the strength of the channel  $XA$  is  $3 \times 10^{-2}$  compared to the channel  $AX$ .

These considerations allow us to develop a very simple model of the overall process [14]:

$$\begin{aligned} \overline{\mathbf{d}}(N) &= \overline{\mathbf{d}_{XX}}(N) + \overline{\mathbf{d}_{AA}}(N) + \overline{\mathbf{d}_{XA}}(N) + \overline{\mathbf{d}_{AX}}(N) \simeq \\ &\simeq \overline{\mathbf{d}_{XX}}(N) + \overline{\mathbf{d}_{AA}}(N) + \overline{\mathbf{d}_{AX}}(N, \Theta_{max}) = \\ &= \overline{\mathbf{d}_{AA}}(N) [1 + R_{AX}] e^{-iE_{AX}\tau(N)} + R_{XX} \end{aligned} \quad (2)$$

The symbol  $\mathbf{d}_{IJ}$  denotes  $N$ -th harmonic component of the laser-induced polarization associated with channel  $IJ$ , i.e. ionization that leaves the ion in the state  $I$  and recombination with the ion in the state  $J$ . The overline denotes orientation-averaged quantities. The complex-valued relative amplitude of the cross-channel,  $R_{AX}$ , is given by orientation-averaged amplitude of the laser-induced transition from the state  $A$  to the state  $X$ . This amplitude takes into account all laser-driven transitions, including the transitions driven by the magnetic field component due to the strong magnetic dipole which couples these states. The cross-channel  $AX$  is maximized in the direction given by the solid angle  $\Theta_{max}$  that optimizes ionization into  $A$  and recombination into  $X$  in the molecular frame. The contribution of the cross-channel is still averaged over all angles in the plane orthogonal to this direction.

In the last equality in Eq.(2), we have written down explicitly the relative phase evolution between the channels  $XX$  and  $AA$ , with  $\tau(N)$  being the time-delay between ionization and recombination and  $E_{AX}\tau(N)$  the difference in the energies between the ionic states  $A$  and  $X$ . Relevant molecular properties including transition matrix elements are described in detail in [14], where we have performed calculations for the single-color elliptical field. Here we use the same input and strategy and only change the single-color elliptical field to the field given by Eq. (1).

According to the calculations of the ionization and recombination amplitudes [14], the relative contribution of the  $XX$  channel,  $R_{XX}$ , is close to unity. We have established [14] that in the single color elliptical field, due to the weakness of the chiral sensitive cross-channels ( $XA$ ,  $AX$ ), these channels can only leave their fingerprint in the high harmonic spectrum near a specific harmonic order, for which the main channels  $XX$  and  $AA$  interfere destructively. The phase term  $E_{AX}\tau(N)$  in Eq.(2) controls this interference.

Following the model in Eq.(2), to estimate chiral dichroism in the two-color elliptically polarized counter-rotating fields, we need to know the ionization  $t_i(N)$  and recombination  $t_r(N)$  times for each harmonic order  $N$ . This allows one to calculate the chiral cross-channel: the amplitude of populating the state  $X$  at the time  $t_r(N)$  after

the ion was created in the state  $A$  at the time  $t_i(N)$ . These times are the well-known solutions of the saddle point equations for high harmonic generation in such two-color fields [36]. Using Eq.(2) we can now evaluate the normalized high harmonic signal vs ellipticity  $\epsilon_1 = \epsilon_2 = \epsilon$  (see Eq.(1)).

Fig. 1 (left panel) shows the calculated chiral dichroism as a function of  $\epsilon = \epsilon_1 = \epsilon_2$ , for  $E_0=0.0239$  a.u. ( $I=2 \times 10^{13}\text{W}/\text{cm}^2$ ) and the carrier frequency  $\omega=0.0224$  a.u. ( $\lambda = 2035$  nm). High values of chiral dichroism are observed in a wide range of harmonic numbers, not only in the region of the destructive interference of the  $XX$  and  $AA$  channels, which is around harmonic 43. Stronger chiral dichroism in this region (about 80 %) as compared to results obtained in weakly elliptical fields (about 3 %) [14] is due to the order of magnitude higher ellipticity ( $\epsilon \sim 0.14$ ).

There are two factors leading to this increase for relatively small ellipticities. Firstly, in the range  $\epsilon \ll 1$ , chiral dichroism is proportional to ellipticity: increasing ellipticity 14 times will respectively increase the chiral dichroism. Secondly, for the field used here, the amplitude of the transition between the states  $A$  and  $X$  is almost two times higher for  $\epsilon \sim 0.14$  than for the single-color field of the same ellipticity.

For higher ellipticities, the disparity between the laser-induced transitions between left and right enantiomers increases and the destructive interference is no longer the decisive mechanism in revealing chiral effects. For example, chiral dichroism at the level of about 20% is found for harmonics 35-51 and ellipticity  $\epsilon_1 = \epsilon_2 = 1$ . Such high values of chiral dichroism are on par with values achievable with PECD method.

The specific value of chiral dichroism for large ellipticities depends on many additional factors. One such factor is the achiral background. Achiral contributions to the harmonic signal are associated [14] with the 'diagonal' HHG channels, involving the cation staying in the same electronic state between ionization and recombination. We found that importance of these channels in cHHG can be controlled via the Stark shift in the two-color field Eq.(1). Specifically, most chiral molecules are polar and have permanent dipoles in the cationic states. Laser interaction with the permanent dipole induces the linear Stark shift. For intense laser fields, these shifts easily approach the  $eV$  scale. Such shifts play important role in laser-induced dynamics in the cation between ionization and recombination. Therefore, they can be used to control cHHG by shaping the laser field in the plane of polarization. This is precisely what is achieved by varying  $\epsilon_1 = \epsilon_2 = \epsilon$  in Eq.(1).

Indeed, for a given electronic state of the cation  $J$  with a permanent dipole  $\mathbf{d}^J$ , the additional phase accumulated in this state due to its interaction with the laser electric field is:

$$\phi_{Stark}^J \propto \int_{t_i}^{t_r} dt E_0 (\epsilon f_x(t) d_x^J + f_y(t) d_y^J). \quad (3)$$

Here  $f_{x,y}(t)$  describe the sub-cycle temporal structure of the electric field in the  $x, y$  polarization plane,  $d_x^J$  and  $d_y^J$  are the corresponding components of the permanent dipole. The amplitude  $d_{JJ}$  of the achiral contribution to the high harmonic field, associated with this state, acquires the corresponding additional phase factor,  $d_{JJ} \propto e^{i\phi_{Stark}^J}$ . In strong

mid-IR fields  $\phi_{Stark}^J \gg 1$ . Thus, the phase term  $\exp(i\phi_{Stark}^J)$  will affect the outcome of coherent averaging of the harmonic response over all molecular orientations, in every channel.

Changing  $\epsilon$  in Eq.(3) changes  $\exp[i\phi_{Stark}^J]$ , which affects coherent averaging over molecular orientations. Fig. 1 (right panel) demonstrates the linear Stark-based ellipticity control of the amplitude of the achiral channel  $AA$  in epoxypropane, using the same theoretical approach as in Ref.[14]. Clearly, we can manipulate the amplitude of this channel within large dynamic range, approaching one order of magnitude in amplitude for the highest harmonics. The channel  $XX$  in epoxypropane shows similar (but not identical) behaviour.

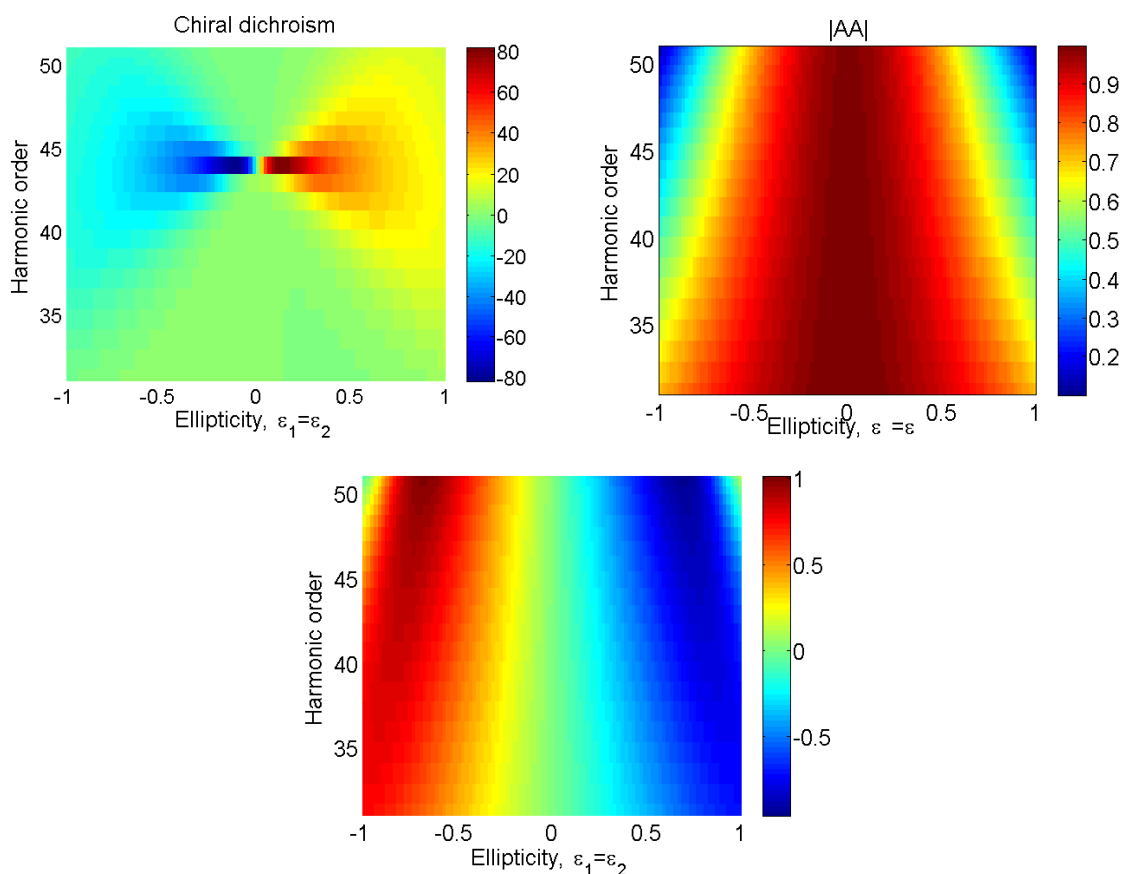


**Figure 1.** HHG in epoxypropane in two-color counter-rotating elliptically polarized fields. Left panel: Estimated chiral dichroism  $Q(N, \epsilon) = 2[Y_S(N, \epsilon) - Y_R(N, \epsilon)]/[Y_S(N, \epsilon) + Y_R(N, \epsilon)]$ , where  $Y_{S,R}$  is the harmonic yield for left (S) and right (R) molecules. The color scale is in percentage. Right panel: The amplitude of  $AA$  channel, coherently averaged in the direction orthogonal to the direction of maximal ionization of the epoxypropane. Bottom panel: Relative phase (between the left and right enantiomer) in radians for the chiral sensitive channel  $AX$  in epoxypropane, without the contribution of the achiral channels. All calculations were done for electric field amplitude  $E_0=0.0239$  a.u. ( $1.24 \times 10^8$  V/cm), fundamental frequency  $\omega=0.0224$  a. u. ( $\lambda = 2035$  nm),  $\epsilon_1 = \epsilon_2 = \epsilon$ .



### 3. Chiral discrimination and chiral dynamic imaging based on HHG spectral and phase measurements

High harmonic spectroscopy gives access to many observables, including harmonic phases [37, 27, 30]. Chiral sensitivity of the harmonic phase has not been explored so far. Fig. 1 (bottom panel) shows the relative phase between the chiral-sensitive transition amplitudes in the cation, for left and right enantiomers. This relative phase is substantial, up to one radian, well within the accuracy of the experimental phase measurements [27]. Thus, cHHG can (and should) also aim at using phase measurements to detect enantiomers. In general, achiral channels may hide this phase. However, here we are assisted by the suppression of achiral background shown in Fig.1 (right panel), which indicates that the enantio-sensitive harmonic phase could be observable for large ellipticities of the driving two-color field, where suppression of the achiral background is strong.

#### 3.1. Detection of the amount of enantiomers in a mixture.

The combination of the harmonic phase measurement with the harmonic spectral measurement brings the new opportunity: *concentration-independent* detection of enantiomeric excess in a mixture  $M$  of left  $S$  and right  $R$  chiral molecules (see Fig.2(a)). Polarization of the medium is proportional to number density. Therefore, accurate determination of enantiomeric excess in chiroptical spectroscopies requires precise determination of number density, which can be very challenging. In the following we show how one can perform the measurement of enantiomeric excess without any knowledge about number densities of the mixture and of pure samples. Suppose we have a mixture of chiral molecules with an overall number density  $N_M$  and the relative fractions of the left-handed and right-handed molecules  $m_S$  and  $m_R$ . Our goal is to find  $\alpha = m_S/m_R$ , which maps into the enantiomeric excess (*e.e.*) as  $e.e. = (1 - \alpha)/(1 + \alpha) \times 25\%$ .

The first step is to measure the harmonic yield from the unknown mixture,  $Y_M(N, \epsilon)$ . Ideally, this should be done for all  $\epsilon$ , changing it from  $\epsilon = 0$  to  $\epsilon = 1$  and then reversing the helicity (denoted as negative  $\epsilon$ ). At the very least, one should measure the yield for, say,  $\epsilon = 1$  and  $\epsilon = -1$ , i.e. perform two spectral measurements.

Next, we use these two measurements to obtain the number density-independent quantity such as the elliptic dichroism,

$$ED_M(N, \epsilon) = 2 \frac{Y_M(N, \epsilon) - Y_M(N, -\epsilon)}{Y_{R,S,M}(N, \epsilon) + Y_{R,S,M}(N, -\epsilon)} \quad (4)$$

or the ratio of the two harmonic intensities

$$\beta_M^2(N, \epsilon) = \frac{Y_M(N, +\epsilon)}{Y_M(N, -\epsilon)}. \quad (5)$$

We can then compare these measurements to the harmonic yields  $Y_{R,S}(N, \epsilon)$  from the samples of pure S (left-handed) or R (right-handed) molecules, also made number

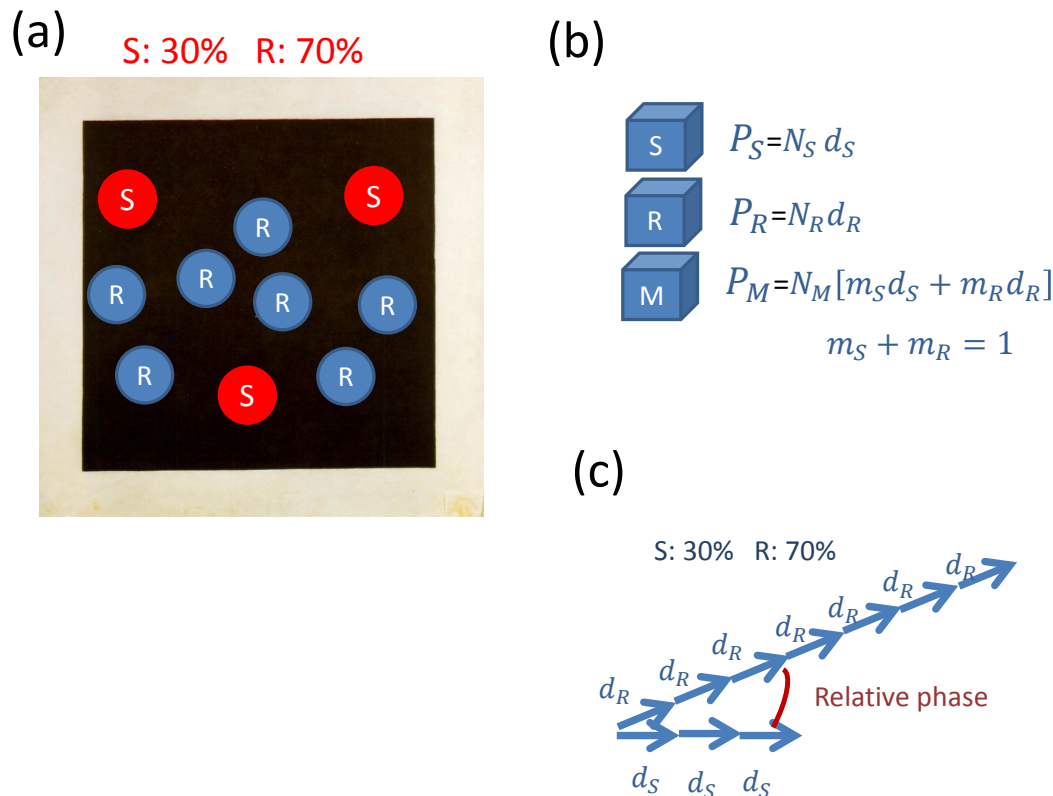


**Figure 2.** Cartoon illustrating importance of the harmonic phase in measuring enantiomeric excess using cHHG. (a) A mixture of 70% right-handed and 30% left-handed molecules. The goal is to find  $\alpha = 0.3/0.7$  (b) Schematic representation of the harmonic response from three gas cells with pure left-handed molecules, pure right-handed molecules, and the unknown mixture. The overall number density of the mixture is  $N_M$ , the relative fractions of the left-handed and right-handed molecules are  $m_S$  and  $m_R$ ,  $P_{R,S,M}$  are the polarizations of the media,  $d_{R,S,M}$  are the harmonic dipoles. (c) In a mixture, the harmonic dipoles from the left-handed and right-handed molecules add coherently, therefore the relative phase between them is crucial for determining  $\alpha = m_S/m_R$  and the enantiomeric excess.

density-independent by measuring the corresponding elliptic dichroisms

$$ED_{R,S}(N, \epsilon) = 2 \frac{Y_{R,S}(N, +\epsilon) - Y_{R,S}(N, -\epsilon)}{Y_{R,S}(N, +\epsilon) + Y_{R,S}(N, -\epsilon)} \quad (6)$$

and/or finding the number density-independent ratios

$$\beta_{R,S}^2(N, \epsilon) = \frac{Y_{R,S}(N, +\epsilon)}{Y_{R,S}(N, -\epsilon)}. \quad (7)$$

For definitiveness, we assume that  $\beta_R > 1$ , i.e. for the R molecules the harmonic yield for  $\epsilon$  is higher than for  $-\epsilon$ .

Suppose we find that for the pure R-sample and, say,  $\epsilon = \pm 1$ , the corresponding elliptic dichroism is  $ED_R(N, \epsilon = 1) = 10\%$ , and for our mixture we have measured

$ED_M(N, \epsilon = 1) = 5\%$ . We also know that for the racemic mixture the dichroism is zero. Can we conclude that our mixture is exactly half-way between pure and racemic? Fig.2 shows why we cannot make such conclusion: the harmonic dipoles from S and R molecules add coherently in the mixture. Thus, the total signal also depends on the relative phase  $\phi_{SR}$  of the harmonic emission between the left-handed and right-handed molecules – the angle between the two harmonic dipoles in Fig.2 (c). This phase can be measured using the two-slit harmonic phase measurement technique developed in [27]. In this case, the measurement should use far-field interference of the harmonic light from two gas cells with enantiomerically pure *S* and *R* molecules. The shift of the interference fringes relative to the case of two identical cells determines the relative phase  $\phi_{SR}$  in a concentration-independent way, with relative concentrations determining fringe contrast but not fringe positions.

Once we have measured  $\phi_{SR}$ , we can use it together with the measured  $\beta_R^2$  and  $\beta_M^2$  to find  $\alpha = m_S/m_R$ . Simple algebra following addition of the harmonic dipoles shows that

$$\beta_M^2 = \frac{\alpha^2 + 2\alpha\beta_R \cos \phi_{SR} + \beta_R^2}{\beta_R^2\alpha^2 + 2\alpha\beta_R \cos \phi_{SR} + 1} \quad (8)$$

Here we have also taken into account that  $|d_S(N, -\epsilon)| = |d_R(N, +\epsilon)|$ .

Varying  $\alpha = m_S/m_R$  between  $\alpha = 0$  (pure R-sample) and  $\alpha = \infty$  (pure S-sample), we see that  $\beta_M$  is squeezed between  $\beta_R > 1$  and  $\beta_S = 1/\beta_R < 1$ , i.e.,  $\beta_S = 1/\beta_R < \beta_M < \beta_R$ .

Next, we re-write the above equation as a quadratic equation for  $\alpha$  and, taking into account that  $\beta_S = 1/\beta_R < \beta_M < \beta_R$ , find its positive solution:

$$\alpha = \frac{-\beta_R \cos \phi_{SR}(\beta_M^2 - 1) + \sqrt{\beta_R^2 \cos^2 \phi_{SR}(\beta_M^2 - 1)^2 + (\beta_R^2 - \beta_M^2)(\beta_R^2\beta_M^2 - 1)}}{(\beta_R^2\beta_M^2 - 1)}. \quad (9)$$

where all quantities depend on the harmonic number,  $N$ , and the ellipticity  $\epsilon$ .

Clearly, the main challenge in this approach stems from the experimental signal to noise ratio, which may result in using small quantities with large error bars. This challenge can be addressed by taking advantage of the huge redundancy of the two-dimensional cHHG measurement, performed for various harmonics  $N$  as a function of  $\epsilon$ . Indeed, every observable used in Eq. (9) depends on two parameters:  $N, \epsilon$ . Therefore, the application of Eq. (9) to every harmonic and every ellipticity should yield exactly the same value of  $\alpha(N, \epsilon) = m_1/m_2$ .

The above scheme includes a set of reference measurements performed on pure samples. Their outcome can be used to characterize multiple samples containing unknown mixtures of left and right molecules, under the same experimental conditions. The additional measurements, specific to the mixture, are the *HHG intensity* measurements yielding elliptical dichroism or  $\beta_M^2(N, \epsilon)$  for the unknown sample.

Crucially, identification of  $\alpha$  using Eq. (9) is concentration-independent: one does not need to know the overall number density of molecules in the pure R-sample, and one does not need to know the overall number density of molecules in the mixture.

*Alternative scheme for detecting enantiomeric excess.* The above measurement scheme for detecting enantiomeric excess is not unique. One can employ two additional phase measurements, specific for the mixture, measuring the relative phase between harmonics emitted by the left-handed molecules and the mixture and the relative phase between the harmonics from the right-handed molecules and the mixture. We now consider such a scheme.

Again, we prepare 3 gas cells: with enantiomerically pure left molecules  $S$ , right  $R$  molecules, and the unknown mixture  $M$ . Using the two-slit technique, we now measure three relative phases: (i) the relative phase between the harmonics generated from the left-handed and the right-handed samples  $\phi_{SR}$ , (ii) between the left-handed molecules and the mixture  $\phi_{MS}$ , and (iii) between the right-handed molecules and the mixture,  $\phi_{MR}$ . We now define number density-independent signals by normalizing the harmonic fields at  $\epsilon \neq 0$  to their values at  $\epsilon = 0$ ,

$$\frac{P_{S,R}(\epsilon)}{P_{S,R}(\epsilon = 0)} = \frac{d_{S,R}(\epsilon)}{d_{S,R}(\epsilon = 0)} \equiv D_{S,R}(\epsilon) \quad (10)$$

Next, we note that

$$\frac{P_M(\epsilon)}{P_M(\epsilon = 0)} = \frac{m_1 d_S(\epsilon) + m_2 d_R(\epsilon)}{m_1 d_S(\epsilon = 0) + m_2 d_R(\epsilon = 0)} = m_1 D_S(\epsilon) + m_2 D_R(\epsilon) \quad (11)$$

since  $m_1 + m_2 = 1$  and  $d_S(\epsilon = 0) = d_R(\epsilon = 0)$ . Here  $D_{R,S}$  are the normalized values of harmonic fields as defined in Eqs. (10,11).

We now show how  $\alpha = m_1/m_2$  can be extracted from the measurements described above. Writing  $D_{S,R} = |D_{S,R}| \exp(i\phi_{S,R})$ , we can explicitly calculate the argument  $\arg[D_M D_R^*] = \phi_{MR}$  in two steps. First,

$$D_M D_R^* = [m_1 D_S + m_2 D_R] D_R^* = m_1 D_S D_R^* + m_2 |D_R|^2. \quad (12)$$

Second, for the quantity  $D_S D_R^*$  in the above equation we write

$$D_S D_R^* = |D_S| |D_R| m_1 [\cos(\phi_{SR}) + i \sin(\phi_{SR})] + m_2 |D_R|^2, \quad (13)$$

Using these two expressions, we finally obtain

$$\tan(\phi_{MR}) = \frac{m_1 |D_S| |D_R| \sin(\phi_{SR})}{m_1 |D_S| |D_R| \cos(\phi_{SR}) + m_2 |D_R|^2}. \quad (14)$$

Analogously, we obtain for  $\phi_{MS}$ :

$$\tan(\phi_{MS}) = -\frac{m_2 |D_S| |D_R| \sin(\phi_{SR})}{m_2 |D_S| |D_R| \cos(\phi_{SR}) + m_1 |D_S|^2}. \quad (15)$$

Introducing the ratio of the spectral amplitudes of the harmonic signals from left and right molecules  $\beta(N, \epsilon) = |D_S(N, \epsilon)|/|D_R(N, \epsilon)|$  and  $\gamma(N, \epsilon) = \frac{|\tan(\phi_{MR}(N, \epsilon))|}{|\tan(\phi_{MS}(N, \epsilon))|}$ , which can be obtained from the phase measurements, we can express  $\alpha = m_1/m_2$  from Eqs. (14,15):

$$\alpha(N, \epsilon) = \frac{\cos(\phi_{SR}(N, \epsilon))(\gamma(N, \epsilon) - 1) + \sqrt{\cos^2(\phi_{SR}(N, \epsilon))(1 - \gamma(N, \epsilon))^2 + 4\gamma(N, \epsilon)}}{2\beta(N, \epsilon)} \quad (16)$$

Again, we note that every observable in Eq. (16) depends on  $N$  and  $\epsilon$ . Therefore, the application of Eq. (16) to every harmonic and every ellipticity should yield exactly the same value of  $\alpha(N, \epsilon) = m_1/m_2$ , thus reducing the signal to noise ratio.

We remind the reader that in this scheme, the independence of the measurement on concentration (number density) arises from normalizing the harmonic response to its value at  $\epsilon = 0$ , see Eqs.(10,11). From now on, all signals will be understood as normalized to their values at  $\epsilon = 0$ , thus explicitly removing their dependence on molecular concentration (number density).

Note that in the second approach we perform redundant spectral measurements by measuring harmonic response for both S- and R-molecules while varying ellipticity in the full range,  $-1 < \epsilon < 1$ , increasing the redundancy of the first scheme by factor two.

### 3.2. Time-resolving sub-femtosecond chiral response in full range of ellipticities

As established in Ref.[14], the main difference between the cHHG signals coming from the two enantiomers is due to the small magnetic-dipole response in the cation. Thus, the multi-electron wavepacket in the cation acquires small correction, which is linear in  $\mu = |\vec{\mu}|$  (a straightforward result of the first order perturbation theory):

$$|\Psi_{R,S}(t)\rangle = |\Psi_0(t)\rangle \pm \mu |\delta\Psi_{ch}(t)\rangle. \quad (17)$$

Here  $|\Psi_0(t)\rangle$  is the time-dependent wavefunction describing the dynamics in the cation in the dipole approximation,  $\pm\mu|\delta\Psi_{ch}(t)\rangle$  is the chiral correction of the time-dependent response, opposite for S and R molecules. This small correction to the multi-electron dynamics in the cation yields chiral correction to the harmonic field

$$D_{R,S}(N, \epsilon) = [D_{R,S}^{(0)}(N, \epsilon) \pm \mu \delta D_{ch}(N, \epsilon)]. \quad (18)$$

Here we have used the number density-independent signals, which can be obtained by normalizing the harmonic fields at  $\epsilon \neq 0$  to their values for  $\epsilon = 0$ ,

$$\frac{P_{S,R}(\epsilon)}{P_{S,R}(\epsilon = 0)} = \frac{d_{S,R}(\epsilon)}{d_{S,R}(\epsilon = 0)} \equiv D_{S,R}(\epsilon) \quad (19)$$

Here  $D_{R,S}^{(0)}(N, \epsilon)$  is the normalized harmonic field in the dipole approximation.

The first-order in  $\mu$  expression is general. Its only assumption is the linear response of the cation to the weak effect of the magnetic field. The dipole  $D_{R,S}^{(0)}(N, \epsilon)$  is not chiral sensitive (once averaged over randomly oriented ensemble),  $D_S^{(0)}(N, \epsilon) = D_R^{(0)}(N, \epsilon) = D^{(0)}(N, \epsilon)$ . The chiral-sensitive component is  $\mu\delta D_{ch}(N, \epsilon)$ . The harmonic yield for left and right enantiomers is then:

$$Y_{R,S}(N, \epsilon) = |D^{(0)}(N)|^2 \left[ 1 \pm 2\mu \frac{|\delta D_{ch}(N)|}{|D^{(0)}(N)|} \cos(\Phi_{ch}(N)) \right]. \quad (20)$$

Using Eq.(20), one obtains for the chiral dichroism  $Q(N, \epsilon) = 2 \frac{Y_S(N, \epsilon) - Y_R(N, \epsilon)}{Y_S(N, \epsilon) + Y_R(N, \epsilon)}$  (the difference between the harmonic yields  $Y_{S,R}(N, \epsilon)$  for left and right molecules divided by the signal from the racemic mixture):

$$Q(N, \epsilon) = 4\mu \frac{|\delta D_{ch}(N, \epsilon)|}{|D^{(0)}(N, \epsilon)|} \cos(\Phi_{ch}(N, \epsilon)). \quad (21)$$

Here  $\Phi_{\text{ch}}$  is the relative phase between the chiral and achiral contributions to the emission amplitude. Thus, the standard measure of the chiral signal, when applied to high harmonic yield, is proportional to  $\mu|\delta D_{\text{ch}}(N, \epsilon)| \cos(\Phi_{\text{ch}}(N, \epsilon))$  – the chiral part of HHG response.

An exciting goal is to separately reconstruct the **amplitude**  $\mu|\delta D_{\text{ch}}(N, \epsilon)|$  and the relative **phase**  $\cos(\Phi_{\text{ch}}(N, \epsilon))$  of the chiral response. This can be done by augmenting the measurement of  $Q(N, \epsilon)$  with two more measurements: (i) of the relative harmonic phase  $\phi_{SR}(N, \epsilon)$  between the  $S$  and  $R$  molecules, and (ii) of the harmonic amplitude in the racemic mixture  $|D^{(0)}(N, \epsilon)|$ .

Eq.(18) allows us to explicitly calculate  $\tan(\phi_{SR})$ :

$$[D^{(0)} - \mu\delta D_{\text{ch}}][D^{(0)} + \mu\delta D_{\text{ch}}]^* \approx |D^{(0)}|^2 + \mu\delta D_{\text{ch}}^* D^{(0)} - \mu\delta D_{\text{ch}} D^{(0)*}, \quad (22)$$

where we have neglected the second order terms in  $\mu$ . Thus,

$$\tan(\phi_{SR}) = 2\mu \sin(\Phi_{\text{ch}}) \frac{|\delta D_{\text{ch}}|}{|D^{(0)}|}. \quad (23)$$

Since the sign of  $\Phi_{\text{ch}}$  becomes important, we specify that  $\Phi_{\text{ch}} = \arg[\delta D_{\text{ch}}^* D^{(0)}]$ . Adding  $\tan(\phi_{SR})^2$  and  $Q^2(N, \epsilon)/4$  we obtain

$$\tan^2(\phi_{SR}(N, \epsilon)) + \frac{Q^2(N, \epsilon)}{4} = W^2(N, \epsilon), \quad (24)$$

where  $W(N, \epsilon)$  gives access to the relative amplitude of the chiral component:

$$W(N, \epsilon) = 2\mu \frac{|\delta D_{\text{ch}}(N, \epsilon)|}{|D^{(0)}(N, \epsilon)|}. \quad (25)$$

The dependence of  $W(N, \epsilon)$  on  $|D^{(0)}(N, \epsilon)|$  can be further eliminated by performing the harmonic measurements in the racemic mixture (rm). Suppose this measurement yields the harmonic spectrum  $y_{rm}(N, \epsilon)$  (also normalized to the signal for  $\epsilon = 0$ ). Then, the amplitude of the chiral component can be obtained as follows:

$$\mu|\delta D_{\text{ch}}(N, \epsilon)| = \frac{W(N, \epsilon)\sqrt{y_{rm}(N, \epsilon)}}{2}. \quad (26)$$

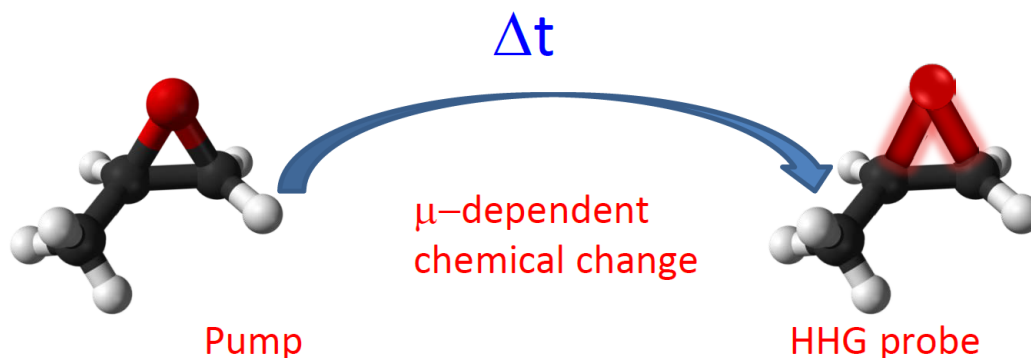
On the other hand, combining Eqs.(21),(25) we obtain the phase between the chiral and achiral components:

$$\cos(\Phi_{\text{ch}}(N, \epsilon)) = \frac{Q(N, \epsilon)}{2W(N, \epsilon)}. \quad (27)$$

Thus, both the amplitude and the relative phase of the chiral signal can be obtained from the combination of spectral and amplitude measurements.

The result described by Eqs.(25,26, 27) is in fact more general than may appear at first glance: Eq.(18) may equally apply to chiral dynamics initiated in a neutral molecule and then probed with HHG. This scheme is sketched in Fig.3. Such pump-probe scheme could allow one to probe the evolution of chiral component  $\mu|\delta D_{\text{ch}}(N, \epsilon)|$  in neutral species during structural changes on a longer, femtosecond time scale. This time scale is determined by the delay between the pump pulse, which excites chiral dynamics in the neutral molecule, and the probe pulse which generates the chiral-sensitive high

harmonic signal. Up to now, no pump-probe time-resolved measurement of ultrafast chirality has been done in the gas phase due to the absence of sufficiently sensitive technique. cHHG promises to open this direction.



$$Q(N, \varepsilon, \Delta t) = 2 \frac{Y_L - Y_R}{Y_L + Y_R} \propto \mu(\Delta t) |\delta D_{ch}(N, \varepsilon, \Delta t)|$$

**Figure 3.** A cartoon of pump-HHG probe measurement describing one of the possible schemes of detecting time-dependent chiral response. The chiral signal in HHG arises from the magnetic dipole. A pump pulse initiates nuclear motion in a chiral molecule. As a result of this motion, the nuclei rearrange themselves around the chiral center. This leads to changing  $\mu$  and therefore changes the high harmonic response induced by the HHG probe. Thus, HHG allows one to follow chiral response from sub fs to fs time scale.

#### 4. Conclusions

Using the example of epoxypropane molecule, we have shown theoretically that cHHG method should strongly benefit from the application of the two-color, counter-rotating elliptically polarized fields. Application of such fields should lead to much higher values of circular dichroism compared to the original scheme [14], which relied on weakly elliptical fields.

We predict that the combination of the harmonic amplitude and phase measurements should allow one to directly measure enantiomeric excess in a concentration-independent way and monitor the evolution of the chiral dynamics with sub-femtosecond time resolution.

We have shown how cHHG method can be used to extract both the amplitude and phase of the chiral signal, for arbitrary configurations of laser fields used to initiate high harmonic process. Indeed, the analysis in Section 3 does not assume any specific field configuration.

We predict that Eqs.(25,26,27) can also be used to extract the amplitude and the phase of the chiral signal from the HHG observables in the pump-probe set-up. In this setup chiral dynamics is first excited in a neutral molecule and then probed with chiral-sensitive high harmonic signal. From single shot to pump-probe, cHHG driven by tailored laser fields thus enables imaging of a wide range of chiral dynamics, with time resolution extended from sub-femtosecond to many tens of femtoseconds.

## Acknowledgments

We thank Prof. M. Ivanov for fruitful discussions. O. S. and S.P. acknowledge the support of the DFG grant SM 292/3-1. O.S. gratefully acknowledges the support of the DFG grant 292/5-1. All authors acknowledge the support of the European COST Action CM1204 XLIC.

## References

- [1] Bonner W A 2000 *Chirality* **12** 114–126
- [2] Shapiro M, Frishman E and Brumer P 2000 *Physical review letters* **84** 1669
- [3] E. Abderhalden, E. Eichwald *Berichte der deutschen chemischen Gesellschaft* **51**, 1312–1322, 1918.
- [4] Tinoco I and Turner D H 1976 *JACS* **98** 6453–6456 (<http://dx.doi.org/10.1021/ja00437a003>) URL <http://dx.doi.org/10.1021/ja00437a003>
- [5] Garcia G A, Nahon L, Daly S and Powis I 2013 *Nature comm.* **4** 1–6 URL <http://dx.doi.org/10.1038/ncomms3132>
- [6] Patterson D, Schnell M and Doyle J M 2013 *Nature* **497** 475–477
- [7] Pitzer M, et al 2013 *Science* **341** 1096–1100 (<http://www.sciencemag.org/content/341/6150/1096.full.pdf>) URL <http://www.sciencemag.org/content/341/6150/1096.abstract>
- [8] Ritchie B 1976 *Phys. Rev. A* **13** 1411–1415
- [9] Böwering N, Lischke T, Schmidtke B, Müller N, Khalil T and Heinzmann U 2001 *Phys. Rev. Lett.* **86**(7) 1187–1190 URL <http://link.aps.org/doi/10.1103/PhysRevLett.86.1187>
- [10] Garcia G A, Nahon L, Lebeck M, Houver J C, Doweck D and Powis I 2003 *The Journal of Chemical Physics* **119** 8781–8784 URL <http://scitation.aip.org/content/aip/journal/jcp/119/17/10.1063/1.1621379>
- [11] Lux C, Wollenhaupt M, Bolze T, Liang Q, Köhler J, Sarpe C and Baumert T 2012 *Angewandte Chemie International Edition* **51** 5001–5005
- [12] Lux C, Wollenhaupt M, Sarpe C and Baumert T 2015 *ChemPhysChem* **16** 115–137 ISSN 1439-7641 URL <http://dx.doi.org/10.1002/cphc.201402643>
- [13] Lehmann C S, Ram N B, Powis I and Janssen M H M 2013 *J. Chem. Phys.* **139** 234307 URL <http://scitation.aip.org/content/aip/journal/jcp/139/23/10.1063/1.4844295>
- [14] Cireasa R, Boguslavskiy A E, B P, Wong M C H, Descamps D, Petit S, Ruf H, Thiré N, Ferré A, Suarez J, Higuete J, Schmidt B E, Alharbi A F, Légaré F, Blanchet V, Fabre B, Patchkovskii S, Smirnova O, Mairesse Y and Bhardwaj V R 2015 *Nat. Phys.* **11** 654 - 658 URL <http://www.nature.com/nphys/journal/v11/n8/full/nphys3369.html>
- [15] Powis I 2008 *Adv. Chem. Phys.* **138** 267–329
- [16] Powis I 2000 *J. Chem. Phys.* **112** 301–310 URL <http://scitation.aip.org/content/aip/journal/jcp/112/1/10.1063/1.480581>
- [17] Fischer P and Hache F 2005 *Chirality* **17** 421



- [18] Fidler A F, Singh V P, Long P D, Dahlberg P D and Engel G S 2014 Nature comm. **5** 3286
- [19] Abramavicius D and Mukamel S 2006 J. Chem. Phys. **124** 034113 URL <http://scitation.aip.org/content/aip/journal/jcp/124/3/10.1063/1.2104527>
- [20] Choi J H, Cheon S, Lee H and Cho M 2008 Phys. Chem. Chem. Phys. **10**(26) 3839–3856 URL <http://dx.doi.org/10.1039/B719263K>
- [21] Ferré A, Handschin C, Dumergue M, Burgy F, Comby A, Descamps D, Fabre B, Garcia G, Géneaux R, Merceron L et al. 2014 Nat. Phot. **8** 93–98
- [22] Fleischer A, Kfir O, Diskin T, Sidorenko P and Cohen O 2014 Nat. Phot. **8** 543–549
- [23] Rhee H, June Y G, Lee J S, Lee K K, Ha J H, Kim Z H, Jeon S J and Cho M 2009 Nature **458** 310–313
- [24] Corkum P B 1993 Phys. Rev. Lett. **71** 1994–1997 URL <http://link.aps.org/doi/10.1103/PhysRevLett.71.1994>
- [25] Schafer K J, Yang B, DiMauro L F and Kulander K C 1993 Phys. Rev. Lett. **70**(11) 1599–1602 URL <http://link.aps.org/doi/10.1103/PhysRevLett.70.1599>
- [26] Baker S, Robinson J S, Haworth C A, Teng H, Smith R A, Chirilă C C, Lein M, Tisch J W G and Marangos J P 2006 Science **312** 424–427
- [27] Smirnova O, Mairesse Y, Patchkovskii S, Dudovich N, Villeneuve D, Corkum P and Ivanov M 2009 Nature **460** 972–977
- [28] Haessler S, Caillat J, Boutu W, Giovanetti-Teixeira C, Ruchon T, Auguste T, Diveki Z, Breger P, Maquet A, Carré B et al. 2010 Nat. Phys. **6** 200–206
- [29] Mairesse Y, De Bohan A, Frasinski L, Merdji H, Dinu L, Monchicourt P, Breger P, Kovačev M, Taïeb R, Carré B et al. 2003 Science **302** 1540–1543
- [30] Bertrand J, Wörner H, Salières P, Villeneuve D and Corkum P 2013 Nat. Phys. **9** 174–178
- [31] Doumy G, Wheeler J, Roedig C, Chirla R, Agostini P and DiMauro L F 2009 Phys. Rev. Lett. **102**(9) 093002 URL <http://link.aps.org/doi/10.1103/PhysRevLett.102.093002>
- [32] Shafir D, Soifer H, Bruner B D, Dagan M, Mairesse Y, Patchkovskii S, Ivanov M Y, Smirnova O and Dudovich N 2012 Nature **485** 343–346
- [33] Smirnova O, Patchkovskii S, Mairesse Y, Dudovich N, Villeneuve D, Corkum P and Ivanov M Y 2009 Phys. Rev. Lett. **102** 063601
- [34] Smirnova O, Patchkovskii S, Mairesse Y, Dudovich N and Ivanov M Y 2009 PNAS **106** 16556–16561 ISSN 0027-8424, 1091-6490 URL <http://www.pnas.org/cgi/doi/10.1073/pnas.0907434106>
- [35] Mairesse Y, Higuët J, Dudovich N, Shafir D, Fabre B, Mével E, Constant E, Patchkovskii S, Walters Z, Ivanov M Y and Smirnova O 2010 Phys. Rev. Lett. **104** 213601 ISSN 0031-9007, 1079-7114 URL <http://link.aps.org/doi/10.1103/PhysRevLett.104.213601>
- [36] Milošević D B and Becker W 2000 Phys. Rev. A **62** 011403
- [37] Paul P M, Toma E S, Breger P, Mullot G, Augé F, Balcou P, Muller H G and Agostini P 2001 Science **292** 1689–1692 ( <http://www.sciencemag.org/content/292/5522/1689.full.pdf> ) URL <http://www.sciencemag.org/content/292/5522/1689.abstract>